AIAA JOURNAL
Vol. 45, No. 7, July 2007

Prediction of Postcontact Parameters of Fluid Droplet Impact on a Smooth Surface

Brett F. Bathel, Neena Stephen,[†] Lukas Johnson,[‡] and Albert Ratner[§]
University of Iowa, Iowa City, Iowa 52242
and
Michael Huisenga[¶]
Iowa State University, Ames, Iowa 50011

DOI: 10.2514/1.24553

Liquid drop impact, spread, and surface coating is critical in wing icing, combustor liner cooling, and other aerospace applications. This study reports an investigation of droplet impact on a smooth quartz surface and formulates new data correlations with extensive error assessment. Several previous models were compared with the experimentally obtained results for droplet maximum spread over a wide range: 1) impact speeds ($1.2 < V < 3.1$ m/s), 2) initial droplet diameter ($2.7 < D < 4.0$ mm), and 3) Reynolds and Weber numbers ($4500 < Re < 13,700$ and $80 < We < 510$). Droplet images were collected using a high-speed digital camera recording at ~2500 frames per second with an image plane spatial resolution of ~16 μm. Based on the large amount of data collected, a statistical analysis was performed to account for error contribution in model prediction and to determine experimental repeatability. Relative mean error in model prediction ranged from 81.3 to 4.0%. Comparison of maximum spread time models with experimental spread times was also made and an improved model that decreases error by a factor of 2 is presented.

I. Introduction

THE study of droplet impact and deformation upon a solid, dry surface is important to a vast range of applications including, but not limited to combustion, aircraft icing, agricultural sprays, mist controlled fuels, ink jet sprays, paint sprays, cooling sprays, fire suppression, and spray coatings. To properly characterize impact and spreading, experimental work must characterize the entire deformation process so as to support and complement computational modeling of the same behavior. Much of the research in the area of droplet impact has provided correlations for predicting the spreading behavior and equilibrium state of fluid droplets on solid surfaces. Particular attention has been given to predicting the maximum spread ratio β_{max} of droplets due to the pervasiveness of this parameter in predictive models. In this study, β_{max} is a nondimensional spreading parameter obtained as calculated as the ratio of the postimpact diameter to the preimpact droplet diameter.

In combustion, such predictive ability lends insight into the breakup behavior of fuel when injected either into a piston chamber or gas turbine combustor. In cooling sprays, the initial deformation of the drops affects the heat transfer from the solid surface into the fluid. Preventative techniques in situations of aircraft icing depend upon an understanding of how water droplets break up and crystallize on wing and body surfaces. Similarly, deformation behavior for fire suppression, agricultural, or ink jet spray droplets dictates the effective surface over which such a fluid can quench a fire, cover a foliar surface, or produce precise characters, respectively. Surface properties, such as porosity and hardness, are also dependent upon the method of application of a spray coating.

One motivation of this study is to improve upon previously obtained data sets by providing a large collection of experimental data taken over a range of impact speeds and droplet diameters. It is then possible to more closely analyze the predictive ability of previously put forth spread models (on a statistical basis) and better quantify the associated error. The ability to perform such an analysis is a result of greatly advanced imaging techniques that have only been realized within the last decade.

Another motivation of this study is to quantify the time-dependent variation in droplet deformation. Although viscous and surface tension effects have been well established as the primary forces responsible for dissipation of preimpact droplet energy, previous experimentation and studies have yet to fully define the variation observed in the characteristic spreading time. Postimpact internal fluid motion and/or surface wave instability are potential culprits to inducing such variation; however, droplet particle-image-velocimetry (PIV) methods detailing intrinsic fluid motion and high-resolution/speed imaging techniques for capturing the appropriate surface wave formation have yet to be realized.

This study employs high-speed digital imagery capable of providing the sizable data set needed to enable thorough statistical analysis of the droplet spread process. The high repeatability of the experiment allows for numerous impact situations having identical preimpact parameters that can be compared against one another to measure in detail the geometric and temporal variability of droplet spread. This work strives to show the differences that arise between previous models when compared against a spectrum of experimental parameters and provides insight into the deformation of a simple Newtonian fluid (water).

Both experimental and computational research efforts in this area have focused on predicting the initial spread phase, point of maximum spread (β_{max}), recoil, and equilibrium state of droplets on solid surfaces. Such efforts have primarily focused on how droplets deform on solid surfaces based upon a set of impact parameters (namely, diameter, velocity, viscosity, contact angle, and surface tension) which are indicative of how preimpact energy is eventually dissipated.

To develop and validate predictive modeling techniques for the spreading process, various experimental imaging methods have been

Received 10 April 2006; revision received 9 March 2007; accepted for publication 12 March 2007.

*Graduate Student, Department of Mechanical and Industrial Engineering, 3131 Seamans Center. Member AIAA.
[†]Undergraduate Student, Department of Biomedical Engineering, 1402 Seamans Center.
[‡]Undergraduate Student, Department of Mechanical and Industrial Engineering, 3131 Seamans Center.
[§]Assistant Professor, Department of Mechanical and Industrial Engineering, 3131 Seamans Center. Member AIAA.
[¶]Graduate Student, Office of Biorenewable Programs.

employed to track the position of the contact line (the point at which solid, liquid, and gas phases meet). The most prevalent method has involved acquiring multiple images at various points in the impact process by means of still photography. By calculating the defining impact parameters, formulation accounting for fluid dynamic effects which retard outward radial flow can be obtained. Typically such formulations apply conservation principles which equate initial kinetic and potential energies with postimpact viscous and surface tension forces and radial inertial energies. Investigations of this manner have been mostly concerned with the final geometries of the deformed droplet, often computationally approximating the flow conditions to replicate simpler processes such as a flattening cylinder or a spherical cap.

Although such methods in modeling have focused purely on the geometric aspects of deformation in relation to energy transfer, they have not been able to account for the time-dependent variations of the same process. Specifically, wave formation, directly proportional to the surrounding ambient gas pressure, can cause oscillations along the surface as a droplet impacts and spreads across a solid. These oscillations ultimately result in varied deformation behavior or even splashing. However, older acquisition techniques have been incapable of capturing such behavior due to the inefficiency of using single photographic images to piece together the deformation process. The primary limitation is that the multi-exposure method cannot provide a continuous look at individual realizations of droplet impact throughout their deformation process. Instead, only general trends could be characterized (such as the influence of contact angle on surface force), and often these trends were formulated by applying only a few experimental cases in which the preimpact parameters were varied.

The ultimate goal of this study is to provide a better prediction of not only the final maximum spread geometries during such impact situations, but to also better characterize the time scales associated with such deformation processes. Specifically, the major aim is to begin quantifying the interplay of ambient pressure and surface wave formation. With the high frame rate (~2500 frames per second), low exposure time (~0.3 ms), and high-resolution (~13–18 μm/pixel) cameras now in use, it is possible to statistically characterize the deformation process in terms of a critical spread time associated with the maximum spread diameter. To the best of the authors' knowledge, few attempts at this type of investigation have been completed primarily due to the imaging limitations discussed. High-speed imaging has been used to examine other droplet-related scientific problems, but there has been no attempt to systematically reexamine the classical droplet impact on a smooth surface problem while examining second-order effects, including surface waves, maximum spread time, and the like. This type of assessment requires a large data set so as to characterize all associated errors. Also, by drawing on this data set, a new model for maximum spread time with half the error rate of the previous best formulation is developed.

II. Review

The physics of droplet behavior has been studied for some time. Experiments by Worthington [1,2] in the late 19th century investigated milk and mercury droplet impact upon a smoked glass surface. The focus of the work was to observe both the splashing patterns of each droplet type upon the solid surface and to detail the deformation period immediately following impact. Initially, a spark flash was used to provide illumination of the deformation process, which was then drawn by hand.

The first numerical investigation of the droplet impact process was performed by Harlow and Shannon [3] in 1967. The complicated equation sets for complex fluid dynamic problems, such as droplet impact and deformation, became tractable with the advent of computers. In their investigation, Harlow and Shannon employed a marker-and-cell technique involving a mesh of computational cells idealized as a viscous, incompressible fluid. For each cell, the nonlinear Navier–Stokes equations were solved and a finite-difference Poisson equation was used to determine pressure.

A full review of the state of droplet dynamic research up to 1993, including impact on both solid and liquid surfaces, was conducted by Rein [4]. The review highlighted formulations for the overall deformation process (Loehr [5]), as well as for the maximum spread ratio, $\beta_{\max}$ (Stow and Hadfield [6], Chandra and Avedisian [7]). Other investigations highlighted in the review concerned the threshold at which droplets would splash, which occurred at a critical impact Weber number, We_c (Stow and Hadfield, and Walzel [8]). As a result of observing the deformation process and final spread diameter $d_{\max}$ of a droplet, several empirical prediction methods have been developed. Typically, an energy balance of some form is used with terms describing both initial and final kinetic, potential, and in some cases, surface energy. The earlier investigations by Stow and Hadfield used this formulation method (Table 1) in deriving their model for the maximum spread ratio $\beta_{\max}$. This ratio, of maximum spread diameter versus initial preimpact droplet diameter, allows for nondimensional consideration, and consequently for relationships to be established between all aspects of the deformation process. The model proposed by Stow and Hadfield took into account the advancing contact angle the deformed drop formed with the contact surface (Fig. 1), which indicated surface properties of the fluid. Their equation, however, did not factor viscous dissipation, resulting in an unbalanced energy equation.

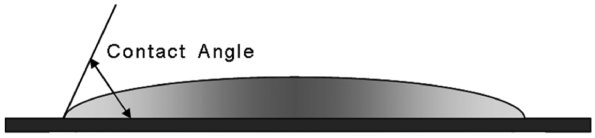

Fig. 1 Liquid–solid contact angle.

Table 1 Literature models for maximum droplet spread ratio $\beta_{\max}$

Author	Model
Stow and Hadfield [6]	$\beta_{\max} = C\sqrt{(2(We + 2We/Fr + 6))/(3(1 - \cos\theta_a))}$
Chandra and Avedisian [7]	$(3We\beta_{\max}^4/2Re) + (\beta_{\max}^2(1 - \cos\theta_a)) - (We/3) - 4 \approx 0$
Asai et al. [17]	$\beta_{\max} = 1 + 0.48\sqrt{We}\exp(-1.48We^{0.22}Re^{-0.21})$
Scheller and Bousfield [18]	$\beta_{\max} = 0.61(Re^2Oh)^{0.166}$
Scheller and Bousfield (FS) [18]	$\beta_{\max} = 0.91(Re^2Oh)^{0.133}$
Pasandideh-Fard et al. [19]	$\beta_{\max} = \sqrt{(We + 12)/(3(1 - \cos\theta_a) + 4(We/\sqrt{Re}))}$
Mao et al. [20]	$[((1 - \cos\theta_a)/4) + (0.2We^{0.83}/Re^{0.33})]\beta_{\max}^3 - ((We + 12)/12)\beta_{\max} + (2/3) = 0$
Fukai et al. [21]	$(We/2Re^{0.772})\beta_{\max}^4 + (2.29(1 - \cos\theta_m))\beta_{\max}^3 - ((We + 12)/3) = 0$
Park et al. [24]	$[((0.33We)/\sqrt{Re}) - (\cos\theta_e/4) + ((1 - \cos\theta_m)/2\sin^2\theta_m)]\beta_{\max}^2 - ((We + 12)/12) + [(\cos\theta_e + 4) - ((1 - \cos\theta_e)/2\sin^2\theta_e)][4\sin^3\theta_e/(2 - 3\cos\theta_e + \cos^3\theta_e)]^{2/3} = 0$
Ukiwe and Kwok [25,26]	$((3(1 - \cos\theta_a)\sqrt{Re} + 4We)/\sqrt{Re})\beta_{\max}^3 - (We + 12)\beta_{\max} + 8 = 0$

A correlation relating the static contact angle to the dynamic contact angle, which is used to assess the surface tension forces acting counter to the radial expansion during deformation, was described by Hoffman [9] and later defined mathematically by Kistler [10].

$$\theta_a = f_{\text{Hoff}}\left[\text{Ca} + f_{\text{Hoff}}^{-1}(\theta_e)\right] \tag{1}$$

where

$$f_{\text{Hoff}}(x) = \cos^{-1}\left\{1 - 2\tanh\left[5.16\left(\frac{x}{1 + 1.31x^{0.99}}\right)^{0.706}\right]\right\} \tag{2}$$

Here, Ca is the capillary number which relates system viscosity to surface tension ($\text{Ca} = \mu V_{\text{CL}}/\sigma$), θ_e is the static (equilibrium) contact angle, and θ_a is the advancing contact angle. The velocity used in calculation of the capillary number is typically the contact line velocity; however, in this experiment the contact line velocity and impact velocity were approximately of the same order, and so the impact velocity was used. Previous work by Roisman et al. [11] has shown that this serves as an effective approximation of advancing contact angle for similar impact conditions.

This formulation was based upon observation of a partially wetting system. The dynamic contact angle behavior was postulated to be dependent upon the static contact angle and capillary number, Ca. It accounted for both the wettability of the fluid on the impact surface and for contact angle hysteresis effects resulting from surface irregularities. More recent investigations into contact line behavior and its relation to droplet impact (for both horizontal and inclined surfaces and varying droplet geometries) are addressed by Cox [12], Bayer and Megaridis [13], Sikalo et al. [14,15], and Vafaei and Podowski [16].

Chandra and Avedisian used an energy balance formulation similar to that of Stow and Hadfield. However, a viscous dissipation term was introduced to explain the inequality encountered in previous attempts to balance the energy equation for the same process.

For all of these studies, surface conditions for the experiment were only described by the advancing contact angle, with the resulting equation for $\beta_{\max}$ being a fourth order polynomial. Asai et al. [17] considered the impact of small ink droplets ($D \approx 44$–81 μm) on a paper surface. In this case, the deformation process was like that of water impacting a solid surface. Absorption of the ink into the paper was considered only after the droplet had reached its maximum spread diameter. From this experiment, the resulting spread ratio $\beta_{\max}$ was observed to be independent of the contact surface and was dependent only on the fluid properties, defined by the nondimensional impact Reynolds and Weber numbers. Experiments by Scheller and Bousfield [18] focused on a mixture of water and glycerin which allowed the viscosity and surface tension of a droplet to be altered. From their testing, it was found that the deformation process of a droplet was dictated by the properties of the fluid alone, rather than by impact velocity. Using the data collected, two equations for $\beta_{\max}$ were developed; the first equation was formulated empirically and the second was formed by using a theoretical cylinder model, which more closely represented the regression of experimental data.

Work by Pasandideh-Fard et al. [19] furthered the work of Chandra and Avedisian by examining the continual evolution of the advancing contact angle throughout the deformation process. It was observed that during the initial phase of spread, the advancing contact angle was consistently observed to be 110 deg. The research also focused on improving the formulation for the viscous dissipation correction W in the energy balance. Both a nondimensional boundary layer thickness δ and nondimensional maximum spread time $\tau_{\max}$ were used to develop a viscous dissipative function φ, which in turn allowed for the calculation of W. Table 2 gives the nondimensional formulations for maximum spread time.

Mao et al. [20] furthered the understanding of viscous dissipation present in droplet impact by considering two instances in which resulting fluid flow outward from an impacting drop would differ. They considered a low-viscosity fluid in which the boundary layer was smaller than that of the water sheet thickness of the deformed drop. Using the work of Chandra and Avedisian and Pasandideh-Fard et al., Fukai et al. [21] solved a set of empirical coefficients applied to a modified equation. With the modified form, it was then possible to further refine the prediction for maximum spread and viscous dissipation.

Table 2 Maximum spread time literature models

Author	Model $\tau = tV/D$
Pasandideh-Fard et al. [19]	$t_{\max} = \frac{8D}{3V}$
Fukai et al. [21]	$t_{\max} = \frac{(D/V)0.680}{Re^{-0.346} + We^{-0.306}(1-\cos\theta_a)^{0.357}}$

Fukai et al. also developed a new term for calculating the maximum spread time. To estimate the time, only spreading up to 90% of the actual maximum was considered to account for error. The reason for this precaution was to account for instances in which the transition of radial expansion to radial retraction was particularly slow (i.e., long, flat portions near maximum spread diameter). Using the 90% nondimensional time fraction, the maximum spread time was then calculated. While the Pasandideh-Fard et al. model consisted of a constant characteristic maximum spread time of 2.67, the Fukai et al. characteristic formulation remained dependent upon initial impact conditions. Additional work by Biance et al. [22] provides a fundamental approach to predicting the inertial phase of spreading occurring $\sim$1 ms into the spreading process and Rioboo et al. [23] examines the entire time evolution of a spreading drop.

Park et al. [24] developed an empirical equation for spreading and recoil at low Weber numbers (≤ 176). Their method considered both the maximum spread and equilibrium conditions of the droplet to determine $\beta_{\max}$. Work completed by Ukiwe and Kwok [25,26] used a high-speed camera system to obtain images of droplets impacting smooth polymer surfaces. The result of the work was a modified form of the Pasandideh-Fard et al. equation for maximum spread.

Work by Renardy et al. [27] details wave formation of occurring immediately after impact on extremely hydrophobic surfaces. More recently, experiments by Xu et al. [28] have detailed the interplay between pressure and a deforming liquid droplet on a solid surface. From the study, it was determined that the surrounding gas pressure strongly influences splashing of a droplet. At elevated pressures, the tendency of a deforming droplet to splash was increased. Conversely, in the presence of a vacuum or low molecular weight gas, it was hypothesized that splashing can be severely limited or even eliminated due to the weak interactions between the gas and expanding fluid sheet.

III. Experimental Arrangement

In this study, 17 and 23-gauge blunt aluminum needles were connected to a 5-gallon Nalgene tank positioned above the impact surface. This configuration allowed for each water droplet to detach from the needle under the influence of pressure from the tank and fall freely to the impact surface. A schematic of the experimental setup is given in Fig. 2.

The impact surface was composed of highly refined NSG (Nippon Silica Glass) "N" material quartz smoothed to $1/4\lambda$ across a 2 in. diameter. This plate served to reduce undesired reflected light from lamps surrounding the impact surface and minimize the effect of surface roughness on the deformation process.

For each needle gauge, the vertical position of the needle was varied to change the impact speed of the drop. For each of nine different fall heights, 70 individual droplet impacts were recorded using a high-speed video system.

Each set of 70 tests was divided into groupings of 10 droplet impacts. Before each grouping was recorded, calibrations were performed to obtain a resolution factor which would be used to calculate all droplet parameters. For all of the tests, the resolution factor was approximately 13–17 μm/pixel. A small number of test drops were also imaged from the top (with the camera at 60 deg to the

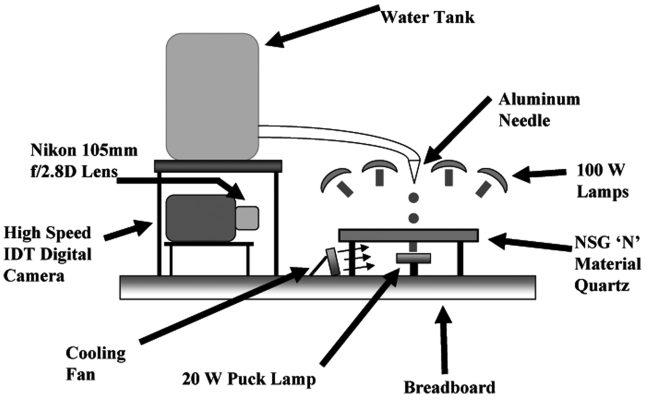

Fig. 2 Experimental setup.

impact plane) to assess postimpact symmetry. No asymmetry was observed, even for the higher impact speed drops.

To capture the continuous video images of the deformation process, an IDT XStream-Vision XS-3 digital video camera was used, operating at approximately 2200 fps. A Nikon® 105 mm $f/2.8$D Micro-Nikkor lens was attached for image enhancement. A droplet impact image sequence is shown in Fig. 3.

The entire video system rested on an optical rail supported by two Newport vibration damping rods. For lighting, four 100-W lamps were positioned around the impact area, and a single 20-W puck lamp was placed beneath the impact surface. The lamps were turned on only during acquisition of the video images, and turned off between tests while the impact surface was cleaned. To further limit the effect of surface heating, a cooling fan was positioned on the breadboard beneath the impact surface. This provided additional heat removal from the impact surface and did not disturb droplets on the top side of the plate. These procedures ensured that the impact surface stayed at a constant temperature.

In the current study, the advancing contact angle θ_a was determined by observation of the deformation period between impact and maximum spread. The static contact angle θ_s was determined from observation of droplets at the static, and the maximum spread contact angle θ_m was calculated by measuring the contact angle at the point of maximum spread after the initial impact. Subsequent radial spread diameters occurring after contact line retraction were not considered. The advancing contact correlation by Hoffman and Kistler was determined by applying the measured static contact angle and calculated capillary number, Ca, based upon the initial impact speed. Whereas calculation of Ca in this study is based upon the preimpact velocity, it would be more appropriate to define this parameter based upon contact line velocity. However, due to the evolving nature of such a velocity, Ca was defined only for the preimpact velocity.

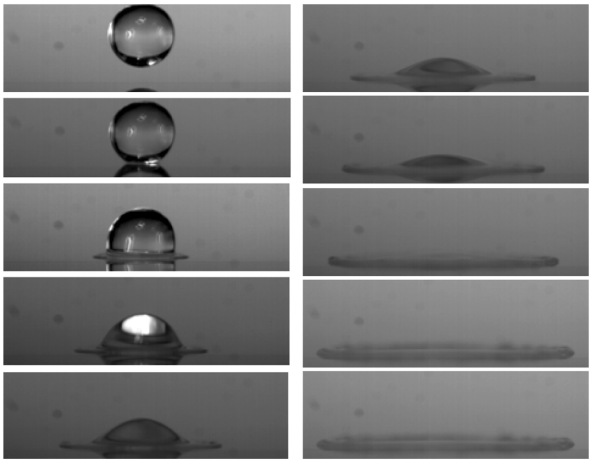

Fig. 3 Image sequence droplet impact.

IV. Procedure

Each droplet impact was video recorded as a series of digital images and the resulting data were extracted from observation of these images. Calibrations were performed by imaging a ruler with millimeter divisions and performing a pixel count across a known distance. The resolution was then calculated by dividing the measured distance by the pixel distance, giving units of μm/pixel.

From the calculation of the resolution factor, crucial parameters such as V, D, $d_{\max}$, We, Re, and Oh could be calculated. To calculate the impact velocity V, the two images before impact were analyzed, and the distance between each position was measured and then divided by the time between frames. Fluid characteristics were obtained by noting the experimental temperature and using published values of viscosity and surface tension for pure water [29].

The method of acquiring the images was straightforward. The flow of water droplets was controlled by a spigot attached to the fluid tank. Pressure from the tank produced single droplets at the needle tip, which then separated under their own weight. A Petri dish was placed below the needle tip to capture the initial stream of droplets. Once a steady flow of droplets was achieved, the dish was removed and the droplet was allowed to impact the surface. This ensured that only slowly formed droplets were analyzed, minimizing error propagation from internal fluid circulation or oscillation resulting from rapid formation.

To measure the maximum spread, static, and advancing contact angles for each of the droplets, images from each droplet height were selected and enhanced using Adobe® Photoshop software. Each of these images was then enlarged, and the contact angles measured. For this study, the entire deformation process, from initial impact to the maximum spread diameter, was examined.

Using the large collection of data obtained through video imaging, 17 groupings of five or more droplets were extracted based on identical values for initial diameters, velocities, Weber, Reynolds, and Ohnesorge numbers. This provided a basis by which a statistical evaluation of the deformation process could be made.

The droplets analyzed in this experiment were such that the difference between the horizontal and vertical preimpact diameters varied by no more than $3.8 \pm 3.0\%$. Error calculations were made by comparing individual model predictions for a given set of preimpact conditions with the averaged experimental parameter for that set. To obtain a root-mean-error value, the average individual errors were then averaged for all preimpact parameters, and the standard deviation of those errors used to tolerance the root-mean-error value:

$$\text{Root Mean Error} = \frac{\left|\sum_{i=1}^{N} \frac{x_i - \bar{x}_{\text{experiment}}}{\bar{x}_{\text{experiment}}}\right|}{\text{N}} \pm S_{\text{Averaged RME}} \qquad (3)$$

Here, x_i was the model prediction of the postimpact parameter of interest, $\bar{x}_{\text{experiment}}$ was the experimental averaged value for the postimpact parameter of interest, N was the total number of identical preimpact parameter data sets, and $S_{\text{Average RME}}$ was the standard deviation of the root mean error for all identical preimpact parameter tests. The $\bar{x}_{\text{experiment}}$ value was obtained by averaging the experimental values of the postimpact parameter of interest. The standard deviation of this value was used to form error bars in the consideration of the characteristic spread time.

V. Experimental Results

A. Characteristic Spread Time Prediction

Both Fukai et al. and Pasandideh-Fard et al. presented nondimensional (Table 1) formulations for determining the maximum spread time required for the impacting droplet to achieve its maximum spread state. Figure 4 compares their formulations compared with the maximum spread times obtained experimentally.

From Fig. 4, it can be seen that both formulations underpredict the maximum spread time. The characteristic spread time predictions by Fukai et al. using the experimentally observed advancing contact angle, Hoffman/Kistler dynamic angle value, and formulation of Pasandideh-Fard et al. resulted in relative mean errors of

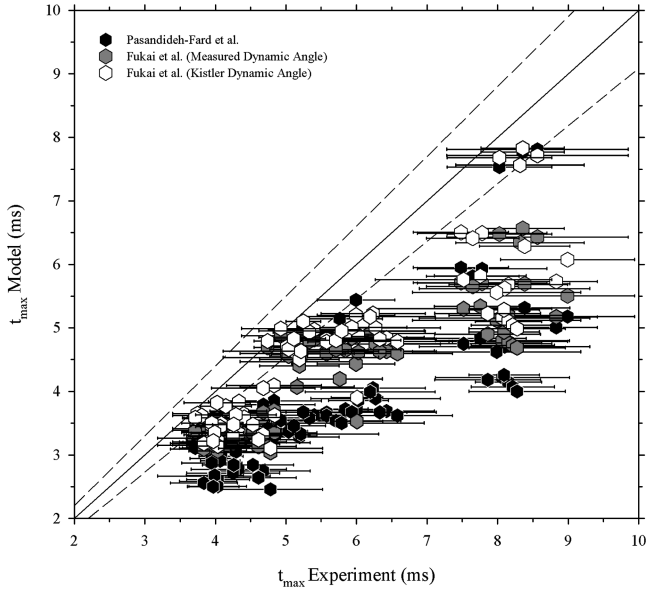

Fig. 4 Comparison of characteristics spread time models.

$23.1 \pm 9.9\%$, $18.0 \pm 9.8\%$, and $31.7 \pm 11.1\%$, respectively. However, it is again noted that formulation by Pasandideh-Fard et al. assumed a constant characteristic spread time.

Figure 4 shows that the model of Fukai et al. tends to exhibit a higher error at lower Reynolds and Weber numbers with decreasing error occurring as transition to higher-end values is made. Pasandideh-Fard et al.'s constant-valued characteristic spread time model exhibits similar error behavior over the range of impact conditions. However, it is observed that as the transition is made from low- to high-end Reynolds and Weber numbers, the relative mean error exhibits a hyperboliclike increase.

Although the relative error of each characteristic model is similar over a range of impact conditions, the prediction by Fukai et al. allows for formula sensitivity to Reynolds and Weber number variations to some extent. This is a more preferable method of spread time prediction due to the applicability of nondimensional formulation to a greater range of defining parameters like preimpact velocity and diameter as well as fluid properties such as viscosity and surface tension. However, the equation considers the effect of advancing contact angle. While this may be applicable in cases where interaction with the impact surface must be carefully considered, it is not necessary in cases where the impacting liquid droplet is not dependent on the impact surface characteristics.

Because of the nondependence of the characteristic spread time on impact surface characteristics, it was desired that a formulation be developed that relied completely on the preimpact conditions of the droplet. By employing a quasi-Newton optimization technique, an equation was formulated that minimized the relative mean error with the experimental data:

$$\tau_{\max} = \left(\frac{4\,Re^{1/5}}{5}\right) + \left(\frac{1}{\sqrt{We}}\right) - \left(\frac{34.75}{1.64(Re \cdot We)^{1/5}}\right) \qquad (4)$$

Figure 5 shows error comparison of the previous literature models with the current model. The curves are a linear best-fit approximation of the error scatter, representing an quasi-average error behavior. The new model exhibits a much lower relative mean error decreased by more than a factor of 2, or $8.9 \pm 7.8\%$.

Figure 6 shows the results of the new model compared with the experimental characteristic maximum spread time. From the figure, it is observed that the model exhibits better predictability of the spread time associated with this type of droplet impact problem. However, it tends to underpredict spread time at approximately 8 ms into the spread phase. Similar underprediction is observed from the previous literature models at this same point. This underprediction occurs around the Reynolds number regime of 9000–10,000 and Weber number regime of 250–300.

Whereas this new characteristic spread time model aids in narrowing the predictive time range in which droplet spread occurs, it still cannot account for the associated statistical deviations evident by the bars in Fig. 6. This behavior suggests that the characteristic spread time is not only a function of the viscosity and surface tension of the fluid, but also of other factors such as ambient pressure. It is hypothesized that such an interaction supports the formation of surface waves (on the air–liquid interface away from the solid substrate) on the radially expanding droplet which eventually becomes unstable as all of the initial kinetic energy is dissipated by viscous and surface forces. These unstable surface waves might then vary interplay between internal fluid motion and surface interactions with the solid surface, ultimately leading to sizable deviations in the characteristic spread time for an impinging droplet. Figure 7 demonstrates more clearly how the droplet impact process (in terms of maximum spread parameters) is more of a time-dependent process rather than a spatially dependent process, as many previous investigations have considered. Indeed, as will be demonstrated in the next section, determination of the maximum geometric

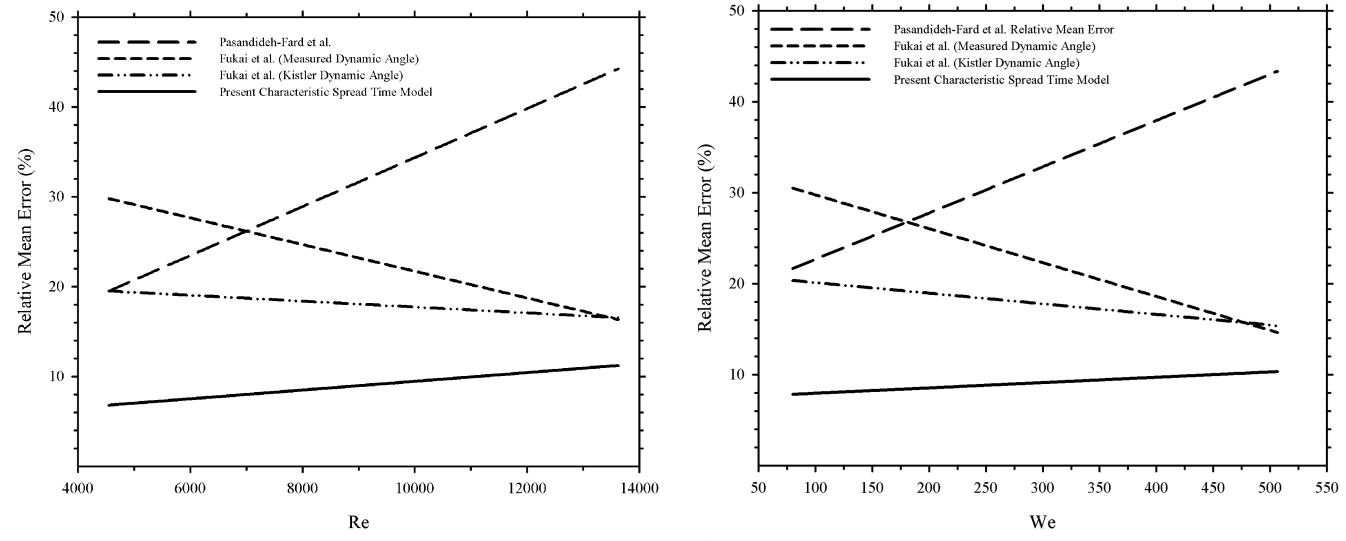

Fig. 5 Relative mean error of characteristic spread time models as functions of a) Reynolds number and b) Weber number.

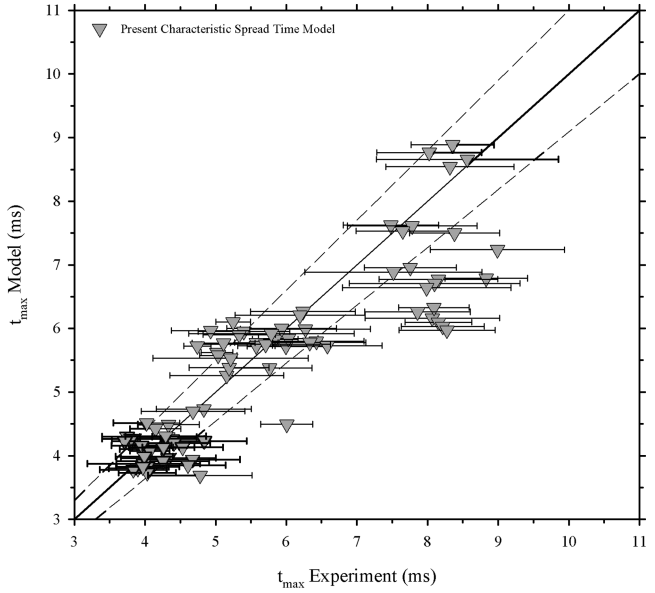

Fig. 6 New characteristic spread time model with 10% error bars.

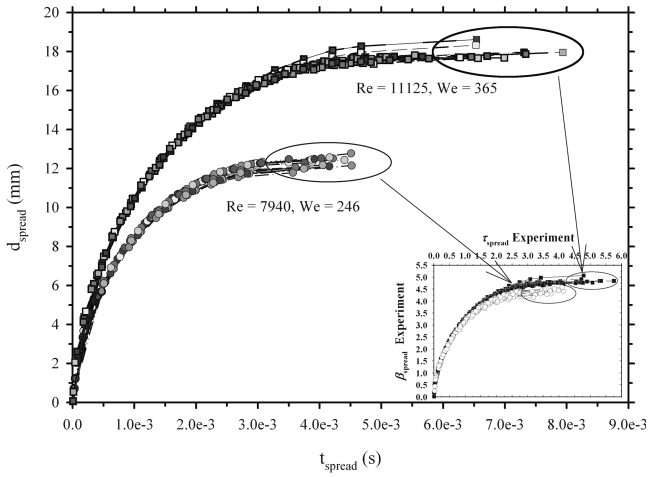

Fig. 7 Dimensional and nondimensional spread diameter evolutions with time. Data represent impact cases with identical nondimensional impact conditions.

characteristics of a deforming droplet has been well established, yet determination of time-sensitive properties remains to be resolved.

B. Prediction of Maximum Spread Diameter

Figures 8a and 8b show the variation of the experimentally obtained maximum spread ratio with the Weber and the Reynolds numbers, respectively. For model comparison, the advancing, maximum, and static contact angles were measured from enlarged sample images, and the resulting experimental average angles achieved were determined to be approximately 88.6 ± 8.4 deg, 54.8 ± 11.1 deg, and 13.4 ± 3.4 deg, respectively. Alternatively, the Hoffman/Kistler model for advancing contact angle was calculated to be $12.6 \pm 6.9\%$ that of the measured advancing contact angle.

The model of Stow and Hadfield's predicted values (using both the Hoffman/Kistler and experimental contact angles) of maximum spread ratio, with a 50% applied correction suggested by the authors, was clearly well outside the error range of the current experiment with relative mean errors of $81.3 \pm 16.7\%$ and $62.7 \pm 23.5\%$ for the model and experimental contact angle cases, respectively.

Chandra and Avedisian improved by more than a factor of 2 on this initial prediction by accounting for viscous dissipation in their formulation. Relative mean error for both the Hoffman/Kistler and

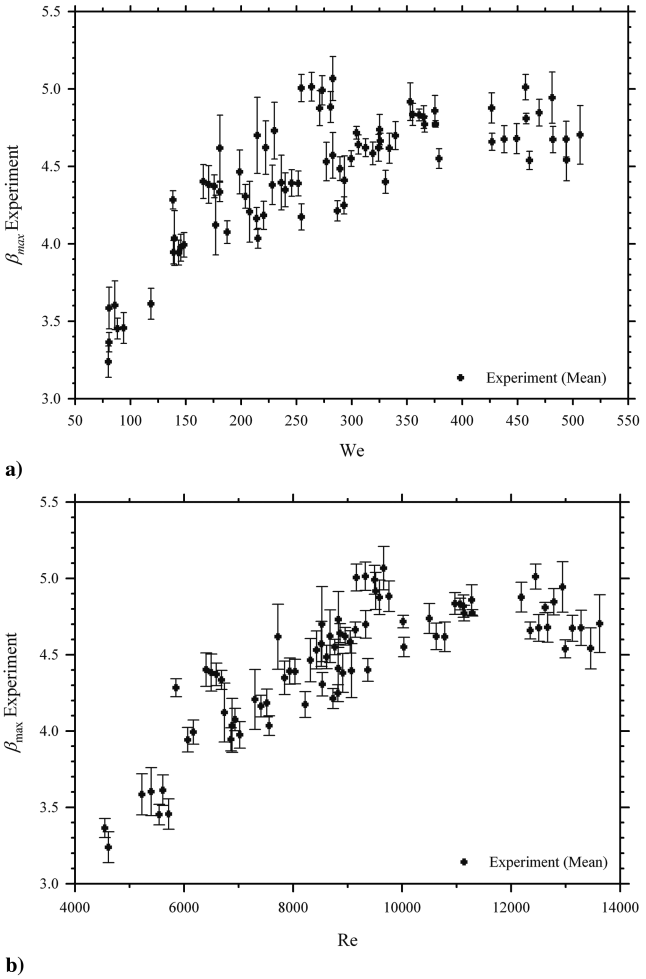

Fig. 8 Experimental maximum spread ratio as a function of a) Weber number and b) Reynolds number.

experimental contact angle cases were observed to be $37.5 \pm 7.5\%$ and $33.5 \pm 7.1\%$, respectively. The model by Fukai et al. exhibited similar magnitudes of error. Application of the experimental advancing contact angle resulted in a relative mean error of $26.9 \pm 5.2\%$ while application of the Hoffman/Kistler angle resulted in a $22.3 \pm 4.2\%$ relative mean error.

Figure 9 shows the formulation by Asai et al. predicted spread ratio within a relative mean error of $8.5 \pm 6.7\%$. This formulation was obtained without the use of a contact angle. For low Reynolds and Weber numbers, the prediction remained within or only deviated slightly from the error interval of the experimentally obtained maximum spread ratio. However, as the lower end of Reynolds and Weber numbers is surpassed, deviation of the model from the experimental results occurs. This is most likely the result of surface tension and viscous effects associated with the higher nondimensional Reynolds and Weber numbers not considered experimentally by Asai et al.

Scheller and Bousfield used a similar approach by obtaining empirical models for the maximum spread ratio. In their model, larger droplets were used to allow for a wider range of Reynolds and Weber numbers to be examined. Figure 8 indicates that their predictions were in good agreement with the experimental β_{max} values over the range of Reynolds and Weber numbers with little discrepancy between the experimental and free spread (FS) models. The resulting relative mean errors for the experimental and free spread models were calculated to be $4.3 \pm 3.3\%$ and $4.4 \pm 3.4\%$, respectively.

The Pasandideh-Fard et al. model using the experimental contact angle predicted spread slightly more accurately than the literature case with a relative mean error of $4.1 \pm 3.3\%$ as compared to $4.7 \pm 3.8\%$.

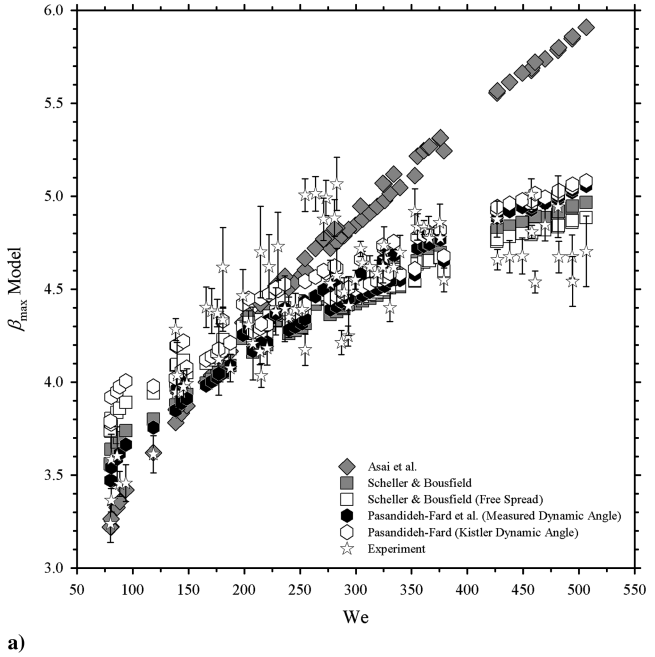

a)

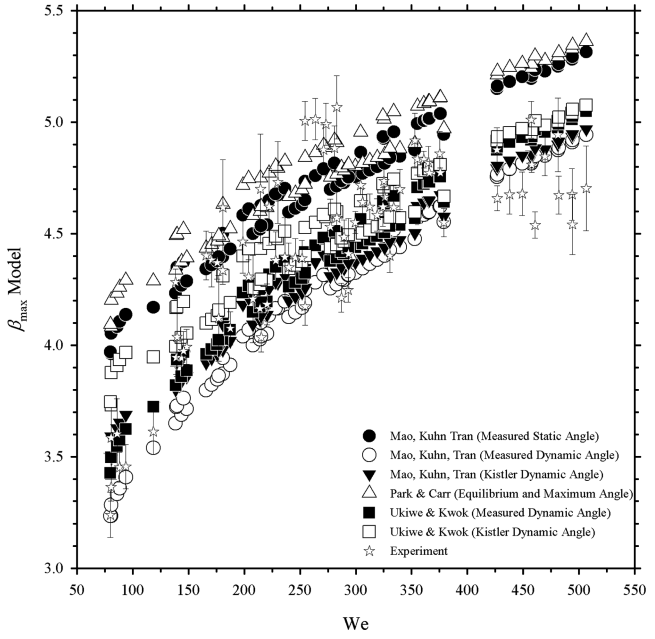

b)

Fig. 9 Model prediction of maximum spread ratio with less than 10% relative mean error versus Weber number.

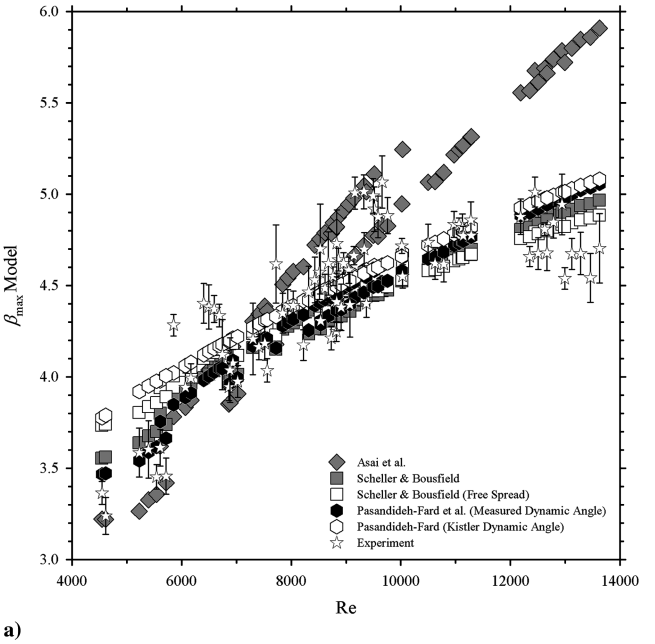

a)

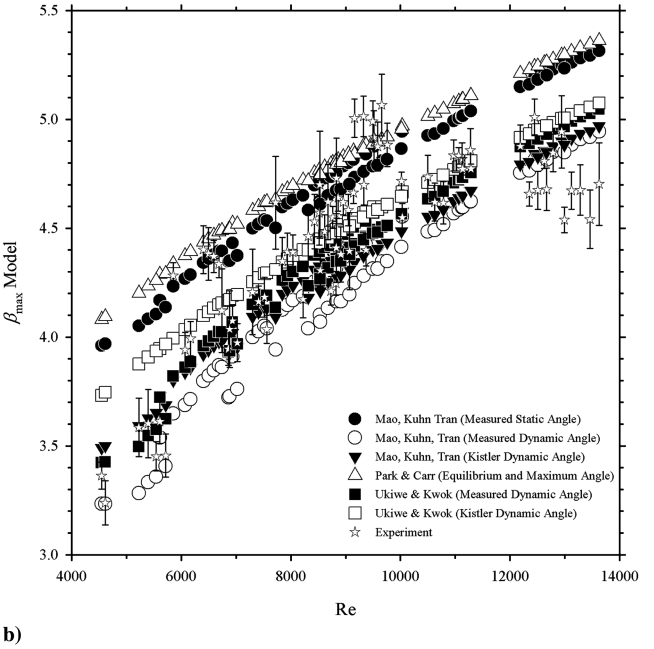

b)

Fig. 10 Model prediction of maximum spread ratio with less than 10% relative mean error versus Reynolds number.

Subsequent models were the result of revisions of earlier spread formulations. These modified equations resulted in a more rigid agreement with the experimental data obtained. The general trend in equation modification tended toward fitting the data to experimental results. This is evident in Figs. 9b and 10b.

Formulation by Mao et al. showed a divergence in predictive ability as the transition from high to low Reynolds and Weber numbers was made. As the transition occurred, the effect of static contact angle in the formulation became more apparent. Application of the Hoffman/Kistler and experimental advancing contact angles resulted in maximum spread ratios that converged toward a single valued β_{max}. Relative mean errors for Hoffman/Kistler advancing contact angle, experimental advancing contact angle, and experimental static contact angle cases were found to be $4.7 \pm 3.4\%$, $5.9 \pm 4.0\%$, and $7.2 \pm 4.9\%$, respectively. Formulation by Park et al. tended to overpredict the maximum spread ratio slightly with a relative mean error of $8.6 \pm 5.9\%$.

The most recent investigation into droplet deformation performed by Ukiwe and Kwok, based on a modified equation by Pasandideh-Fard et al., resulted in a relative mean error of $4.1 \pm 3.3\%$ using the experimental advancing contact angle and $4.6 \pm 3.6\%$ using the Hoffman/Kistler advancing contact angle.

Although the calculated relative mean error is only a simple indicator of model agreement with the experimental results, it does provide for selection of the more agreeable models. Based on the relative mean errors, the models of Scheller and Bousfield, Pasandideh-Fard et al., Mao, Kuhn, Tran (with Hoffman/Kistler contact angle), and Ukiwe and Kwok provide for the best agreement. Each provided relative mean errors of less than 5%. Figure 10 shows all models exhibiting less than 10% relative mean error with the experimental data of this study. Figure 11 provides a direct comparison of the maximum spread models with less than 10% error relative to the experimental results.

It should be noted that although the most recent models predict maximum spread ratio to within a very small percentage of error,

some discrepancies still exist due to unknown factors. This is evident in Figs. 6 and 7. As β_{max} varies over the range of Weber and Reynolds numbers, the values oscillate instead of following a more linear trend. Because of the smooth surface employed in this experiment, it is assumed that fluid-surface interactions are negligible. This again supports the possibility that certain instability modes, which have been qualitatively examined but not quantified, can describe this occurrence. Specifically, the internal fluid motion resulting in fluid oscillation and fluid-vapor interaction at the fluid surface causing fluid oscillation.

Whereas consideration of the fluid oscillation for low-speed impact situations would only improve maximum spread prediction by a small amount, translation of the low-speed impact case to higher-speed impact cases will certainly need to include consideration of fluid oscillation to accurately predict breakup and subsequent droplet formation.

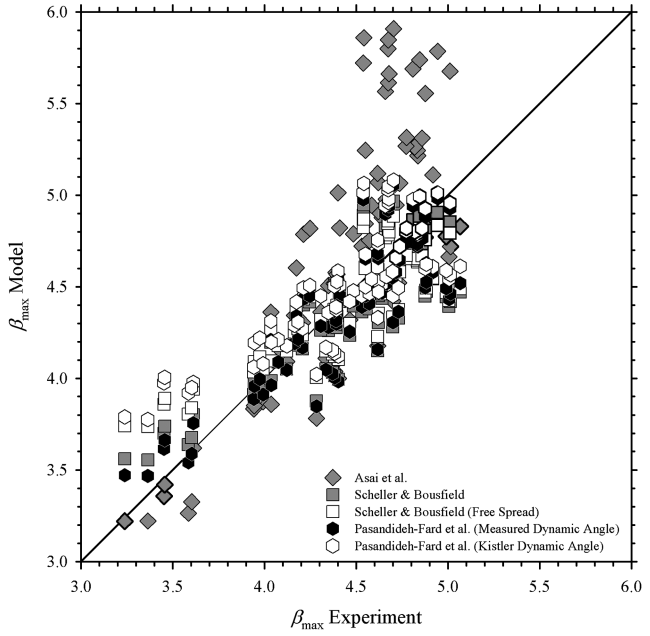

a)

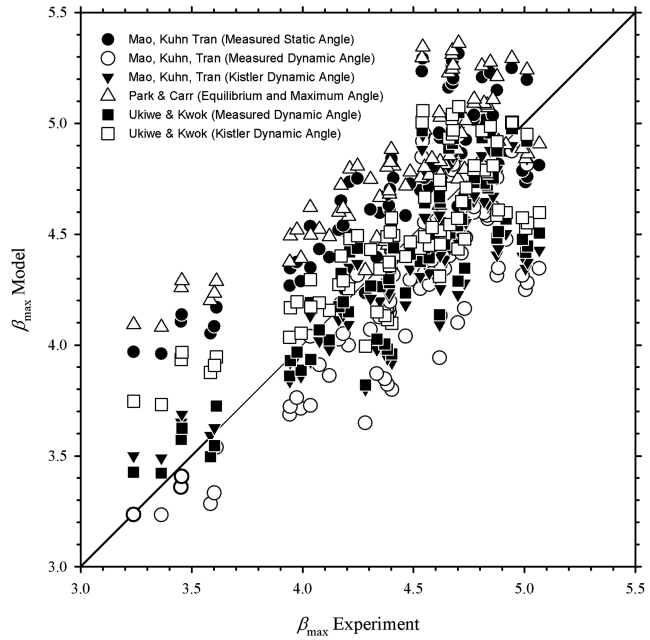

b)

Fig. 11 Comparison with maximum spread models with experiment (less than 10% relative mean error).

C. Effect of Contact Angle

Every model, except for those put forth by Asai et al. and Scheller and Bousfield, implemented the static, equilibrium, maximum, or advancing contact angle to some extent. Although in most cases the models continued to accurately predict the maximum spread ratio within a small percentage of error, the contact angles used remained without a solid definition.

Considering the models of Pasandideh-Fard et al. and Mao et al., no notable difference was observed between the Hoffman/Kistler and experimental contact angle cases, except for small variation at lower Reynolds and Weber numbers. For the range of preimpact parameters tested the effect of contact angle, in general, was not a real contributing factor to the prediction of maximum spread. Therefore, due to the specific range of preimpact parameters tested, it is observed that the dominant physical properties include fluid viscosity and surface tension. Analysis of contact angle provides little insight in regard to this type of impact problem and it is other issues, such as those discussed above (i.e., internal fluid motion, surface wave formation and instability, and solid-fluid surface interaction) that should be examined thoroughly so that a true mechanistic definition droplet impingement can be made.

VI. Conclusions

The large data set produced in this study was employed first to examine the accuracy of existing models for the impact of a Newtonian fluid onto a smooth, dry surface, with the findings being that these models predict the maximum spread to within 5% of the actual value. It was also shown, for the range of parameters and experimental conditions considered herein, that use of contact angle provided no improvement in prediction accuracy.

The maximum spread time prediction models examined exhibited deviation from experiment which most likely was the result of secondary physical (including surface instability) mechanisms that alter the characteristic spread time behavior of impinging droplets. These mechanisms can be expected to play a greater role at higher ambient or stagnation pressures, while for the cases examined here the impact was less than the total model uncertainty of 8.9%. To effectively model the entire spread process from the initial point of impact to the point of maximum spread, a time-dependent function needs to be formulated which can include these mechanisms and predict spread trends over a large range of Reynolds and Weber numbers. Based on this work, it appears that a formulation that captures energy transfer into and out of surface waves, wave behavior, and bulk fluid circulation would be able to predict drop spreading and maximum spread time with significantly greater accuracy. Such a formulation would also provide a mechanism-based path to splash prediction. It appears that such a model is also necessary if higher impact or spread velocity situations are to be addressed.

For lower Reynolds and Weber number impacts, the results of this paper and the work of recent investigators provide a solid basis for prediction of maximum spread distance and time. Therefore, these results can be applied to simplify modeling of the entire spread process under such conditions.

Acknowledgments

The authors would like to thank NASA and the FAA for sponsoring this research, the University of Iowa for its continued support, and program manager Virendra Sarohia of the NASA Jet Propulsion Laboratory for his assistance.

References

[1] Worthington, A. M., "On the Forms Assumed by Drops of Liquids Falling Vertically on a Horizontal Plate," *Proceedings of the Royal Society of London*, Vol. 25, June 1876, pp. 261–271.

[2] Worthington, A. M., "A Second Paper on the Forms Assumed by Drops of Liquids Falling Vertically on a Horizontal Plate," *Proceedings of the Royal Society of London*, Vol. 25, Jan. 1877, pp. 498–503.

[3] Harlow, F. H., and Shannon, J. P., "The Splash of a Liquid Drop,"

Journal of Applied Physics, Vol. 38, No. 10, 1967, pp. 3855–3866.
[4] Rein, M., "Phenomena of Liquid Drop Impact on Solid and Liquid Surfaces," *Fluid Dynamic Research*, Vol. 12, Aug. 1993, pp. 61–93.
[5] Loehr, K. F., and Lasek, A., "Splashing of Drops," *Archive of Applied Mechanics*, Vol. 42, Nos. 4–5, 1990, pp. 507–513.
[6] Stow, C. D., and Hadfield, M. G., "An Experimental Investigation of Fluid Flow Resulting from the Impact of a Water Drop with an Unyielding Dry Surface," *Proceedings of the Royal Society of London, Series A: Mathematical and Physical Sciences*, Vol. 373, No. 1755, 1981, pp. 419–441.
[7] Chandra, S., and Avedisian, C. T., "On the Collision of a Droplet with a Solid Surface," *Proceedings of the Royal Society of London: Mathematical and Physical Sciences*, Vol. 432, No. 1884, 1991, pp. 13–41.
[8] Walzel, P., "Zerteilgrenze Beim Tropfenprall," *Chemie Ingenieur Technik*, Vol. 52, No. 4, 1980, pp. 338–339.
[9] Hoffman, R. L., "A Study of the Advancing Interface I. Interface Shape in Liquid-Gas Systems," *Journal of Colloid Interface Science*, Vol. 50, Feb. 1975, pp. 228–235.
[10] Kistler, S. F., "Hydrodynamics of Wetting," *Wettability*, Vol. 49, Marcel Dekker, New York, 1993, pp. 311–429.
[11] Roisman, I. V., Rioboo, R., and Tropea, C., "Normal Impact of a Liquid Drop on a Dry Surface: Model for Spreading and Receding," *Proceedings of the Royal Society of London A*, Vol. 458, No. 2022, 2002, pp. 1411–1430.
[12] Cox, R. G., "Inertial and Viscous Effects on Dynamic Contact Angle," *Journal of Fluid Mechanics*, Vol. 357, Feb. 1998, pp. 249–278.
[13] Bayer, I. S., and Megaridis, C. M., "Contact Angle Dynamics in Droplets Impacting on Flat Surfaces with Different Wetting Characteristics," *Journal of Fluid Mechanics*, Vol. 558, July 2006, pp. 415–449.
[14] Sikalo, S., Wilhelm, H. D., Roisman, I. V., Jakirlic, S., and Tropea, C., "Dynamic Contact Angle of Spreading Droplets: Experiments and Simulations," *Physics of Fluids*, Vol. 17, No. 6, 2005, pp. 62103-1–62103-13.
[15] Sikalo, S., Tropea, C., and Ganic, E. N., "Dynamic Wetting Angle of a Spreading Droplet," *Experimental Thermal and Fluid Science*, Vol. 29, July 2005, pp. 795–802.
[16] Vafaei, S., and Podowski, M. Z., "Analysis of the Relationship Between Liquid Droplet Size and Contact Angle," *Advances in Colloid and Interface Science*, Vol. 113, Nos. 2–3, 2005, pp. 133–146.
[17] Asai, A., Shioya, M., Hirasawa, S., and Okazaki, T., "Impact of an Ink Drop on Paper," *Journal of Imaging Science and Technology*, Vol. 31, No. 2, 1993, pp. 205–207.
[18] Scheller, B. L., and Bousfield, D. W., "Newtonian Drop Impact with a Solid Surface," *American Institute of Chemical Engineers Journal*, Vol. 41, No. 6, 1995, pp. 1357–1367.
[19] Pasandideh-Fard, M., Qiao, Y. M., Chandra, S., and Mostaghimi, J., "Capillary Effects During Droplet Impact on a Solid Surface," *Physics of Fluids*, Vol. 8, No. 3, 1996, pp. 650–659.
[20] Mao, T., Kuhn, D. C. S., and Tran, H., "Spread and Rebound of Liquid Droplets upon Impact on Flat Surfaces," *American Institute of Chemical Engineers Journal*, Vol. 43, No. 9, 1997, pp. 2169–2179.
[21] Fukai, J., Tanaka, M., and Miyatake, O., "Maximum Spreading of Liquid Droplets Colliding with Flat Surfaces," *Journal of Chemical Engineering Japan*, Vol. 31, No. 3, 1998, pp. 456–461.
[22] Biance, A. L., Christophe, C., and Quere, D., "First Steps in the Spreading of a Liquid Droplet," *Physical Review E (Statistical Physics, Plasmas, Fluids, and Related Interdisciplinary Topics)*, Vol. 69, No. 12, 2004, pp. 16301-1–16301-4.
[23] Rioboo, R., Marengo, M., and Tropea, C., "Time Evolution of Liquid Drop Impact onto Solid, Dry Surfaces," *Experiments in Fluids*, Vol. 33, July 2002, pp. 112–124.
[24] Park, H., Carr, W. W., Zhu, J., and Morris, J. F., "Single Drop Impaction on a Solid Surface," *American Institute of Chemical Engineers Journal*, Vol. 49, No. 10, 2003, pp. 2461–2471.
[25] Ukiwe, C., and Kwok, D. Y., "On the Maximum Spreading Diameter of Impacting Droplets on Well-Prepared Solid Surfaces," *Langmuir*, Vol. 21, Jan. 2005, pp. 666–673.
[26] Ukiwe, C., Mansouri, A., and Kwok, D. Y., "The Dynamics of Impacting Water Droplets on Alkanethiol Self-Assembled Monolayers with Co-Adsorbed CH_3 and CO_2H Terminal Groups," *Journal of Colloid and Interface Science*, Vol. 285, May 2005, pp. 760–768.
[27] Renardy, Y., Popinet, S., Duchemin, L., Renardy, M., Zaleski, S., Josserand, C., Drumright-Clarke, M. A., Richard, D., Clanet, C., and Quere, D., "Pyramidal and Toroidal Water Drops After Impact on a Solid Surface," *Journal of Fluid Mechanics*, Vol. 484, June 2003, pp. 69–83.
[28] Xu, L., Zhang, W. W., and Nagel, S. R., "Drop Splashing on a Dry Smooth Surface," *Physical Review Letters*, Vol. 94, No. 18, 2005, pp. 1–4.
[29] Crowe, C. T., Elger, D. F., and Roberson, J. A., *Engineering Fluid Mechanics*, 7th ed., Wiley, Hoboken, NJ, 2001.

S. Aggarwal
Associate Editor